

# Single Image Dehazing by Multi-Scale Fusion

Codruta Orniana Ancuti and Cosmin Ancuti

**Abstract**—Haze is an atmospheric phenomenon that significantly degrades the visibility of outdoor scenes. This is mainly due to the atmosphere particles that absorb and scatter the light. This paper introduces a novel single image approach that enhances the visibility of such degraded images. Our method is a fusion-based strategy that derives from two original hazy image inputs by applying a white balance and a contrast enhancing procedure. To blend effectively the information of the derived inputs to preserve the regions with good visibility, we filter their important features by computing three measures (weight maps): luminance, chromaticity, and saliency. To minimize artifacts introduced by the weight maps, our approach is designed in a multiscale fashion, using a Laplacian pyramid representation. We are the first to demonstrate the utility and effectiveness of a fusion-based technique for dehazing based on a single degraded image. The method performs in a per-pixel fashion, which is straightforward to implement. The experimental results demonstrate that the method yields results comparative to and even better than the more complex state-of-the-art techniques, having the advantage of being appropriate for real-time applications.

**Index Terms**—Single image dehazing, outdoor images, enhancing.

## I. INTRODUCTION

OFTEN, the images of outdoor scenes are degraded by bad weather conditions. In such cases, atmospheric phenomena like haze and fog degrade significantly the visibility of the captured scene. Since the aerosol is misted by additional particles, the reflected light is scattered and as a result, distant objects and parts of the scene are less visible, which is characterized by reduced contrast and faded colors.

Restoration of images taken in these specific conditions has caught increasing attention in the last years. This task is important in several outdoor applications such as remote sensing, intelligent vehicles, object recognition and surveillance. In remote sensing systems, the recorded bands of reflected light are processed [1], [2] in order to restore the outputs. Multi-image techniques [3] solve the image dehazing problem by processing several input images, that have been taken in different atmospheric conditions. Another alternative [4] is to assume that an approximated 3D geometrical model of the scene is given. In this paper of Treibitz and Schechner [5]

Manuscript received August 3, 2011; revised June 5, 2012, October 13, 2012, and January 13, 2013; accepted March 5, 2013. Date of publication May 13, 2013; date of current version June 11, 2013. The associate editor coordinating the review of this manuscript and approving it for publication was Prof. Wai-Kuen Cham.

The authors are with the Expertise Center for Digital Media, Hasselt University, Diepenbeek 3590, Belgium (e-mail: codruta.ancuti@uhasselt.be; cosmin.ancuti@uhasselt.be).

Color versions of one or more of the figures in this paper are available online at <http://ieeexplore.ieee.org>.

Digital Object Identifier 10.1109/TIP.2013.2262284

different angles of polarized filters are used to estimate the haze effects.

A more challenging problem is when only a single degraded image is available. Solutions for such cases have been introduced only recently [6]–[10].

In this paper we introduce an alternative single-image based strategy that is able to accurately dehaze images using only the original degraded information. An extended abstract of the core idea has been recently introduced by the authors in [11]. Our technique has some similarities with the previous approaches of Tan [7] and Tarel and Hautière [10], which enhance the visibility in such outdoor images by manipulating their contrast.

However, in contrast to existing techniques, we built our approach on a fusion strategy. We are the first to demonstrate the utility and effectiveness of a fusion-based technique for dehazing on a single degraded image. Image fusion is a well studied process [12], that aims to blend seamlessly several input images by preserving only the specific features of the composite output image. In this work, our goal is to develop a simple and fast technique and therefore, as will be shown, all the fusion processing steps are designed in order to support these important features. The main concept behind our fusion based technique is that we derive two input images from the original input with the aim of recovering the visibility for each region of the scene in at least one of them. Additionally, the fusion enhancement technique estimates for each pixel the desirable perceptual based qualities (called weight maps) that controls the contribution of each input to the final result. In order to derive the images that fulfill the visibility assumptions (good visibility for each region in at least one of the inputs) required for the fusion process, we analyze the optical model for this type of degradation. There are two major problems, the first one is the color cast that is introduced due to the airlight influence and the second is the lack of visibility into distant regions due to scattering and attenuation phenomena.

The first derived input ensures a natural rendition of the output, by eliminating chromatic casts that are caused by the airlight color, while the contrast enhancement step yields a better global visibility, but mainly in the hazy regions. However, by employing these two operations, the derived inputs taken individually still suffer from poor visibility (e.g. analyzing figure 3 it can be easily observed that the second input restores the contrast of the hazy inputs, but at the cost of altering the initial visibility of the closer/haze-free regions).

Therefore, to blend effectively the information of the derived inputs, we filter (in a per-pixel fashion) their important features, by computing several measures (weight maps). Consequently, in our fusion framework the derived inputs

are weighted by three normalized weight maps (luminance, chromatic and saliency) that aim to preserve the regions with good visibility.

Finally, to minimize artifacts introduced by the weight maps, our approach is designed in a multi-scale fashion, using a Laplacian pyramid representation of the inputs combined with Gaussian pyramids of normalized weights.

Our technique has several advantages over previous single-image dehazing methods. First, our approach performs an effective per-pixel computation, different from the majority of the previous methods [6]–[8] that process patches. A proper per-pixel strategy reduces the amount of artifacts, since patch-based methods have some limitations due to the assumption of constant airlight in every patch. In general, the assumptions made by patch-based techniques do not hold, and therefore additional post processing steps are required (e.g. the method of He et al. [8] needs to smooth the transmission map by alpha-matting). Secondly, since we do not estimate the depth (transmission) map, the complexity of our approach is lower than most of the previous strategies. Finally, our technique performs faster which makes it suitable for real-time applications. Even compared with the recent effective implementation of Tarel and Hautière [10] our technique is able to restore a hazy image in less time, while showing more visually plausible results in terms of colors and details (see figure 1).

Our technique has been tested extensively for a large set of different hazy images (the reader is referred to the supplementary material). Results on a variety of hazy images demonstrate the effectiveness of our fusion-based technique. Moreover, we perform a quantitative experimental evaluation based on the measure of Hautière et al. [13]. The main conclusion is that our approach is less prone to artifacts, yielding very similar results with the physically-based techniques such as the technique of Fattal [6], He et all. [8], Nishino et al. [14] and Kopf et al. [4]. We believe that this is a key advantage of our technique.

The rest of paper is structured as follows. In the next section, the related techniques that deal with haze removal are briefly reviewed. In Section III, we discuss some theoretical aspects of light propagation in such environments. In Section IV, we introduce our new single image based dehazing technique; the details regarding our fusion technique are discussed in this section. In the next section we report and discuss the results while in Section VI our method is summarized.

## II. RELATED WORK

Enhancing images represents a fundamental task in many image processing and vision applications. As a particular challenging case, restoring hazy images requires specific strategies and therefore an important variety of methods have emerged to solve this problem.

Firstly, several dehazing techniques have been developed for remote sensing systems, where the input information is given by a multi-spectral imaging sensor installed on the Landsat satellites. The recorded six-bands of reflected light are processed by different strategies in order to yield enhanced output images. The well-known method of Chavez [1] is suitable for homogeneous scenes, removing the haze by subtracting an offset value determined by the intensity distribution



Fig. 1. Comparison with the fast method of Tarel and Hautière [10]. Our method performs faster and yields more visually plausible results than [10]. Notice the sky and sea regions.

of the darkest object. Zhang et al. [15] introduced the haze optimized transformation (HOT), using the blue and red bands for haze detection, that have been shown to be more sensitive to such effects. Moro and Halounova [2] generalized the dark-object subtraction approach [1] for highly spatially-variable haze conditions.

A second category of methods, employs multiples images or supplemental equipment. In practice, these techniques use several input images taken in different atmospheric conditions. Different medium properties may give important information about the hazy image regions. Such methods [3], [16], [17] produce pleasing results, but their main drawback is due to their acquisition step that in many cases is time consuming and hard to carry out.

Different strategies have been developed when the approximated 3D geometrical model of the scene is given. The forerunner method of Narasimhan and Nayar [18] employs an approximated depth-map specified interactively by the users. Hautière et al. [19] designed a method for vehicle vision systems, where weather conditions are first estimated and then used to restore the contrast according to a scene structure which is inferred a priori. The *Deep Photo* [4] system uses the existing georeferenced digital terrain and urban models to restore foggy images. The depth information is obtained by iteratively aligning the 3D models with the outdoor images.

Another class of techniques exploits the properties of the airlight that is partially polarized [5], [20]–[23]. By using different angles of polarized filters the resulting images of the same scene can be processed to estimate the haze effects. The difference between such images enables the estimation of the magnitude of the polarized haze light component. These methods have shown less robustness for scenes with dense haze where the polarization light is not the major degradation factor.

However, a more difficult case is when only a single hazy image is used as an input information. The single image dehazing is an ill-posed problem that can be solved by different strategies [6]–[8], [10], [14] that have been introduced only recently. Roughly, these methods can be divided into contrast-based and statistical approaches. Tan's [7] method belongs to the first category. In this case the image restoration maximizes the local contrast while constraining the image intensity to be less than the global atmospheric light value. The contrast-based enhancing approach of Tarel and Hautière [10] has shown to be a computationally effective technique, but

assumes as well that the depth-map must be smooth except along edges with large depth jumps. Regarding to the second category, the technique of Fattal [6] employs a graphical model that solves the ambiguity of airlight color. It assumes that image shading and scene transmission are locally uncorrelated. He et al. [8] built their approach on the statistical observation of the dark channel [1], that allows a rough estimation of the transmission map. To refine the final depth-map, the transmission map values are extrapolated into the unknown regions, by a relatively computationally expensive matting strategy [24]. The technique of Kratz and Nishino [9], recently extended [14], is a Bayesian probabilistic method that jointly estimates the scene albedo and depth from a single degraded image by fully leveraging their latent statistical structures. Their approach models the image with a factorial Markov random field in which the scene albedo and depth are two statistically independent latent layers, which are estimated jointly.

Our method is also a single image dehazing technique. Different than previous single image dehazing approaches, our technique is built on the principle of image fusion, a well-studied topic of computational imaging that has found many useful applications such as interactive photomontage [25], image editing [26], image compositing [27], [28] and HDR imaging [29], [30]. The main idea is to combine several images into a single one, retaining only the most significant features. Even though the fusion principle has been used previously to restore hazy images, but using additionally near-infrared (NIR) image of the same scene [31], we are the first that introduce a single image dehazing technique based on the fusion principle that blends only the information existing in the input image. Our strategy bears some similarity with the recent methods of He et al. [8] and Tarel and Hautière [10]. Both of these methods can be seen as filtering solutions since the dark channel [8] can be related with an erosion problem, while [10] employed their defined *median of median filter* in order to preserve both edges and corners. However, our approach is fundamentally different since it removes the haze by simply blending the two derived inputs weighted by several measures. Our strategy combines the input information in a per-pixel fashion minimizing the loss of the image structure by a multi-scale strategy. While no post-processing steps are required it is also straightforward to implement and computationally effective.

### III. BACKGROUND THEORY: LIGHT PROPAGATION

Due to the absorption and scattering, the light crossing the atmosphere is attenuated and dispersed. While in normal conditions (clear day) the size of air molecules is relatively small compared with the wavelength of visible light, the scattering influence might be considered insignificant. As the title discloses, in this paper we are dealing with special atmosphere conditions due to the presence of haze. Discussed in the study of McCartney [32], haze is traditionally an atmospheric phenomenon where dust, smoke and other dry particles obscure the clarity of the sky. Haze reduces visibility for distant regions by yielding a distinctive gray hue in the

captured images. As will be demonstrated, our algorithm is able to deal as well with a particular case: foggy scenes. Fog is a dense cloud of water droplets, or cloud, that is close to the ground. In general, this phenomena appears when night conditions are clear but cold, and the heat released by the ground is absorbed during the day. As the temperature of the ground decreases, it cools the air above it to the dew point forming a cloud of water droplets known as radiation fog.

Based on the Koschmieder's [33] law only a percentage of the reflected light reaches the observer causing poor visibility in such degraded scenes. The light intensity  $\mathcal{I}$  for each pixel  $x$ , that reaches the observer is described by two main additive components: *direct attenuation* and *veiling light*, also known as *airlight*:

$$\mathcal{I}(x) = \mathcal{J}(x) T(x) + V_\infty (1 - T(x)) \quad (1)$$

where  $\mathcal{J}$  is the scene radiance or haze-free image,  $T$  is the *transmission* along the cone of vision and  $V_\infty$  is the *veiling* color constant. The optical model assumes linear correlation between the reflected light and the distance between the object and observer. The first component, *direct attenuation*  $\mathcal{D}$ , represents how the scene radiance is attenuated due to medium properties:  $\mathcal{D}(x) = \mathcal{J}(x) T(x)$ . The *veiling light* component  $\mathcal{V}$  is the main cause of the color shifting, being expressed as:

$$\mathcal{V}(x) = V_\infty (1 - T(x)) \quad (2)$$

The value of  $T$  depicts the amount of light that has been transmitted between the observer and the surface. Assuming a homogeneous medium, the transmission  $T$  is determined as  $T(x) = e^{(-\beta d(x))}$  with  $\beta$  being the medium attenuation coefficient due to the scattering, while  $d$  represents the distance between the the observer and the considered surface. Practically, the problem is to estimate from the hazy input  $\mathcal{I}$  the latent image  $\mathcal{J}$  when no additional information about depth and airlight are given.

## IV. FUSION-BASED DEHAZING

In this section is presented in detail our fusion technique that employs only the inputs and weights derived from the original hazy image. The fundamental idea is to combine several input images (guided by the weights maps) into a single one, by keeping only the most significant features of them. Obviously, the choice of inputs and weights is application-dependent. By processing appropriate weight maps and inputs, we demonstrate that our fusion-based method is able to effectively dehaze images.

### A. Inputs

As mentioned previously, the input generation process seeks to recover optimal region visibility in at least one of the images.

In practice, there is no enhancing approach that is able to remove entirely the haze effects of such degraded inputs. Therefore, considering the constraints stated before, since we process only one captured image of the scene, the algorithm generates from the original image only two inputs that recover color and visibility of the entire image. The first one better

depicts the haze-free regions while the second derived input increases visible details of the hazy regions.

Inherently inspired by the previous dehazing approaches such as Tan [7], Tarel and Hautière [10] and He et al. [8], we searched for a robust technique that will properly white balance the original image. Our **first input**  $I_1$  is obtained by white balancing the original hazy image. By this step we aim a natural rendition of images, by eliminating chromatic casts that are caused by the atmospheric color.

In the last decades many white balancing approaches [34]–[38] have been proposed in the literature (a systematic overview of the existing methods is presented in [39]). Several specialized techniques have been experimented in the context of our problem. Since we aim for a computationally effective dehazing approach, we opted for the *shades-of-gray* color constancy technique [37]. Despite of its simplicity, this low-level approach of Finlayson and Trezzi [37] has shown to yield comparable results to those of more complex white balance algorithms (that produces reliable results based on natural image statistics [40]). The main objective of white balance algorithms, is to identify the illuminant color  $e(\lambda)$  or its projection on the RGB color channels ( $R_e, G_e, B_e$ ). We use the same notations as in the original manuscript of Weijer and Gevers [41] of *grey-edges* that is just an extension of *shades-of-gray*. Unfortunately, we observed that the *grey-edges* technique often failed when processing hazy images. We believe that this is due to the lack of local contrast in the hazy regions but also since the hazy images are characterized by a smaller amount of edges.

Given an image  $f$ , for a Lambertian surface, the intensity measured can be modeled as:

$$f(x) = \int_{\omega} e(\lambda)s(\lambda, x)c(\lambda)d\lambda \quad (3)$$

where  $e(\lambda)$  is the radiance given by the light source,  $\lambda$  is the wavelength,  $s(\lambda, x)$  denotes the surface reflectance,  $c(\lambda) = [R(\lambda), G(\lambda), B(\lambda)]$  describes the sensitivity of the sensors while  $\omega$  is the visible spectrum.

The illuminant  $\mathbf{e}$  to be estimated, is expressed as:

$$\mathbf{e} = (R_e, G_e, B_e) = \int_{\omega} e(\lambda)c(\lambda)d\lambda. \quad (4)$$

According to the *Grey-World* assumption of Buchsbaum [34] the average reflectance of the scene is achromatic (gray). This hypothesis is mathematically defined as follows:

$$\frac{\int s(\lambda, x)dx}{\int dx} = \kappa \quad (5)$$

where  $\kappa$  is the constant assumed to have the value 0.5.

Next, by replacing  $s$  in equation 3 with 5, the following expression is obtained:

$$\begin{aligned} \frac{\int f(x)dx}{\int dx} &= \frac{1}{\int dx} \int \int_{\omega} e(\lambda)s(\lambda, x)c(\lambda)d\lambda dx \Leftrightarrow \\ \frac{\int f(x)dx}{\int dx} &= \kappa \int_{\omega} e(\lambda)c(\lambda)d\lambda \end{aligned} \quad (6)$$

As shown in *shades-of-gray* [37] and *grey-edges* [41], white balance can be defined based on Minkowski norm of

images. *Grey-World* [34] algorithm estimates the illumination, by stating that the average color of the entire image raised to a power  $n$  is achromatic (gray).

$$\left[ \frac{\int f^n dx}{\int dx} \right]^{\frac{1}{n}} = \kappa \mathbf{e} = \kappa (R_e, G_e, B_e) \quad (7)$$

As demonstrated, *shades-of-gray* is part of the same family with *Grey World* [34] and *max-RGB* [35] techniques. This is easy to demonstrate by setting norm  $n = 1$  and  $n \rightarrow \infty$  respectively in the equation 7. For *shades-of-gray* approach  $n$  can take any number between 1 and  $\infty$  (default value is set to  $n = 6$ ). When  $n = 1$ , all the components from the scene contribute uniformly to the average. When  $n$  is increased, the impact of the components is directly proportional with their intensity.

Since the first input  $I_1$  shows good visibility in non-hazy regions and discards the color shifting, the second input  $I_2$  is generated from this  $I_1$  in order to enhance the contrast in those regions that suffer due to the airlight influence.

For the **second input** we searched for a relatively complementary processing technique, capable to enhance those regions that present low contrast. Considering the airlight factor from the optical model (eq. 2) (that is both additive and multiplicative with the transmission), and since the haze is dominant in the hazy images, it is expected that the hazy regions would have a great influence over the average of the image. Moreover, due to the fact that the airlight influence increases linearly with the distance, the luminance of these regions is assumed to amplify with the distance. In practice, based on these observations, second input  $I_2$  is obtained automatically by subtracting the average luminance value of the entire image  $I$  from the original image  $I$ . This operation has the effect of amplifying the visibility in regions degraded by haze, but yields some degradation in the rest of the image (the effect of this conversion is shown in figure 3). A similar effect may be obtained by general contrast enhancing operators (e.g. gamma correction, histogram stretching) that also amplify the visibility in the hazy parts, while destroying the details in the rest of the image. However, this degradation is detected and solved in our fusion approach by defining proper weight maps (please refer to the next subsection and figure 3).

Mathematically, the second input computed for each pixel  $x$  is obtained by applying the following expression:

$$I_2(x) = \gamma (I(x) - \bar{I}) \quad (8)$$

where  $\gamma$  is a factor that increases linearly the luminance in the recovered hazy regions (default value is  $\gamma = 2.5$ ). This default value for  $\gamma$  matches for those most cases. However, in our experiments there are few exceptions that are not satisfied. These cases are characterized by the fact that hazy regions are relatively darker than non-hazy regions (see figure 7). Since fusion blends selectively (guided by the weight maps) the two inputs, the results of the dehazing operation will suffer also by darker aspect (some algorithms suffer from such problems as can be noticed by a closed inspection of figure 8 of [7], in figure 1 of [10] or in figure 6 of [14]). To generate optimal results for these cases, we derived a general expression for

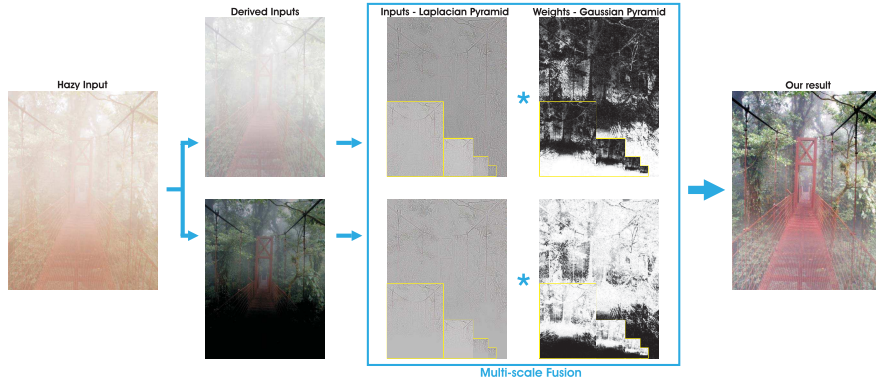


Fig. 2. Overview of our technique. From the input hazy image are derived two enhanced versions. These two derived inputs are weighted by three normalized weight maps (luminance, chromatic and saliency) - here we show only the Gaussian of corresponding normalized maps. Finally, the Laplacian of the inputs and Gaussian of the weights are blended in a multi-scale fashion that avoids introducing artifacts. In this outline we depict our approach by using only 5 ( $I = 5$ ) scale levels in the Laplacian and Gaussian spaces.

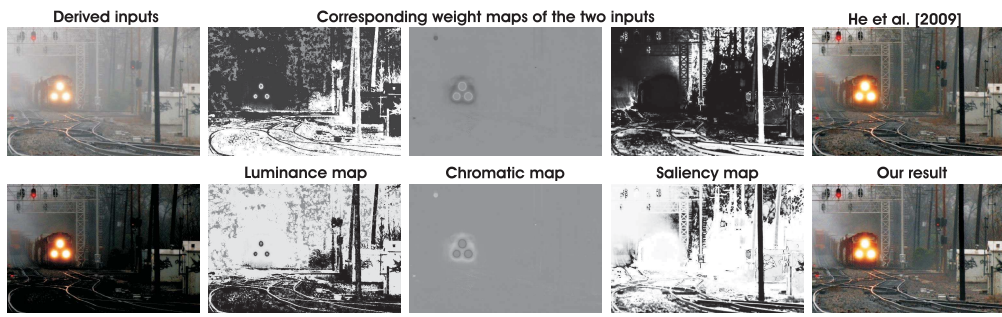


Fig. 3. Derived inputs and weight maps. In the left side the two derived inputs are shown. In the middle are displayed the three weight maps corresponding to the inputs. Finally, in the right column the results of He et al. [8] and our result are shown.

*gamma* ( $\gamma = 2(0.5 + \bar{I})$ ), that is correlated with the average luminance of the image (we employ this information, since  $\bar{I}$  is a good indicator of the image brightness appearance). The parameter *gamma* has a similar impact as the tone mapping stage of [10] that has been applied on the the haze-free regions, assumed to be in the bottom third part of the original image.

### B. Weight Maps

As can be seen in figures 2 and 3, by applying only these enhancing operations, the derived inputs still suffer from low visibility mainly in those regions with dense haze and low light conditions. The idea that global contrast enhancement techniques are limited to dealing with hazy scenes has been remarked previously by Fattal [6]. This is due to the fact that the optical density of haze varies across the image and affects the values differently at each pixel. Practically, the limitation of the general contrast enhancement operators (e.g. gamma correction, histogram equalization, white balance) is due to the fact that these techniques perform (constantly) the same operation across the entire image. In order to overcome this limitation, we introduce three measures (weight maps). These maps are designed in a per-pixel fashion to better define the spatial relations of degraded regions.

Our weight maps balance the contribution of each input and ensure that regions with high contrast or more saliency from a derived input, receive higher values.

The ***luminance weight map*** measures the visibility of each pixel and assigns high values to regions with good visibility

and small values to the rest. Since hazy images present low saturation, an effective way to measure this property is to evaluate the loss of colorfulness. This weight is processed based on the *RGB* color channel information. We make use of the well known property, that more saturated colors yield higher values in one or two of the color channels. This weight map is simply computed (for each input  $I_k$ , with  $k$  indexes the derived inputs) as the deviation (for every pixel location) between the *R*, *G* and *B* color channels and the luminance *L* from the input:

$$W_L^k = \sqrt{1/3 [(R^k - L^k)^2 + (G^k - L^k)^2 + (B^k - L^k)^2]} \quad (9)$$

Since the luminance *L* is computed by averaging the *RGB* channels, this disparity yields higher values for the saturated pixels which are assumed to be part of the initial haze-free regions. On the other hand, because haze produces colorlessness and low contrast, this measure will assign small values (reducing the contribution of these locations to the output) for the hazy but also for the deteriorated regions (e.g. in the second derived input we refer to the regions that have lost their luminance and therefore have a dark appearance). As illustrated in figure 3, the  $W_L$  map is a straightforward, yet effective identification of such regions.

The luminance weight acts as an identifier of the degradation induced in  $\mathcal{I}_2$  in the haze-free regions, ensuring a seamless transition between the derived inputs  $\mathcal{I}_1$ ,  $\mathcal{I}_2$ . On the other hand this map also tends to reduce the global contrast

and colorfulness. To overcome these effects, in our fusion framework we define two additional weight maps: a chromatic map (colorfulness) and a saliency map (global contrast).

The **chromatic weight map** controls the saturation gain in the output image. This weight map is motivated by the fact that in general humans prefer images characterized by a high level of saturation. Since the color is an inherent indicator of the image quality, often similar color enhancement strategies are also performed in tone mapping.

To obtain this map, for each pixel the distance between its saturation value  $S$  and the maximum of the saturation range is computed as following:

$$\mathcal{W}_C^k(x) = \exp\left(-\frac{(S^k(x) - S_{max})^2}{2\sigma^2}\right) \quad (10)$$

where  $k$  indexes the derived inputs, the default value of the standard deviation is  $\sigma = 0.3$  and  $S_{max}$  is a constant that depends by the color space employed (in our approach we opted for the *HSI* color space and higher saturated pixels correspond to  $S_{max} = 1$ ). Therefore, small values are assigned to pixels with reduced saturation while the most saturated pixels get high values. As a result, this map ensures that the initial saturated regions will be better depicted in the final result.

The **saliency weight map** identifies the degree of conspicuousness with respect to the neighborhood regions. This perceptual quality measure assesses that a certain object/person stands out from the rest of the image, or from nearby regions. In general, saliency (also referred to as *visual attention* [42], [43]) no matter what the motivation behind it (biologically based [44], [45], computational [43] or combination of both), seeks to estimate the contrast of image regions relative to their surroundings (based on different image features such as intensity, color or orientation).

For this measure, we use the recent saliency algorithm of Achanta et al. [45]. This strategy is inspired by the biological concept of center-surround contrast. The saliency weight at pixel position  $(x, y)$  of input  $I^k$  is defined as:

$$\mathcal{W}_S^k(x) = \|I_k^{\omega_{hc}}(x) - I_k^\mu\| \quad (11)$$

where  $I_k^\mu$  represents the arithmetic mean pixel value of the input  $I_k$  (a constant value during the entire process that is computed only once) while  $I_k^{\omega_{hc}}$  is the blurred version of the same input that aims to remove high frequency such as noise.

$I_k^{\omega_{hc}}$  is obtained by employing a small  $5 \times 5$  ( $\frac{1}{16}[1, 4, 6, 4, 1]$ ) separable binomial kernel with the high frequency cut-off value  $\omega_{hc} = \pi/2.75$ . For small kernels, the binomial kernel is a good approximation of its Gaussian counterpart, but it has the advantage that in this way it can be computed more efficiently. Once the blurred version of the image  $I_k^{\omega_{hc}}$  and the arithmetic mean  $I_k^\mu$  are computed, the saliency is obtained in a per pixel fashion. We opted for the approach of Achanta et al. [45] since this technique is computationally efficient. Moreover, it is able to produce maps with well-defined boundaries and uniformly highlighted salient regions (even at high resolution scales). These features of this saliency map, prevent introducing unwanted artifacts in the result image yielded by our fusion technique since neighboring comparable values

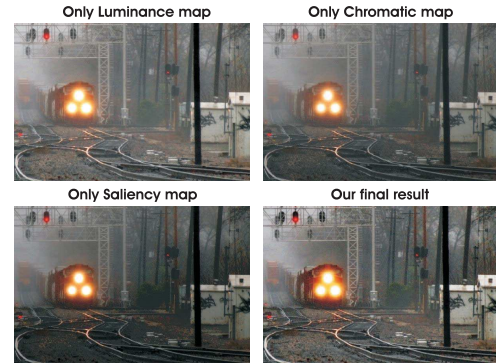


Fig. 4. Impact of each weight map to the final result. Results of our fusion technique but using only one weight map at a time.

are assigned similarly on the saliency map. Additionally, the employed map [45] emphasizes large regions and estimates uniform values for the whole salient regions. As a result, the effect of this gain is to enhance the global and local contrast appearance (that corresponds to large scale). As can be observed in figure 4, one of the main effects of this measure is to increase the contrast in highlighted and shadowed regions.

By processing a large and diverse set of degraded images, we observed that the impact of these three measures is, in general, equally important. However, the first measure has the highest impact on the visibility. To better understand the contribution of each of these weight maps, the reader is referred to figure 4 that displays a result processed with our fusion technique, but using only one weight map at a time.

The resulted weights  $\mathcal{W}^k$  are obtained by multiplying the processed weight maps  $\mathcal{W}_L^k$ ,  $\mathcal{W}_C^k$ ,  $\mathcal{W}_S^k$ . To yield consistent results, we normalize the resulted weight maps ( $\bar{\mathcal{W}}^k(x) = \mathcal{W}^k(x)/\sum_k \mathcal{W}^k(x)$ ). This operation constrains that sum at each pixel location  $x$  of the normalized weight maps to equal one.

### C. Multi-Scale Fusion

In the fusion process, the inputs are weighted by specific computed maps in order to conserve the most significant detected features. Each pixel  $x$  of the output  $\mathcal{F}$  is computed by summing the inputs  $\mathcal{I}_k$  weighted by corresponding normalized weight maps  $\mathcal{W}^k$ :

$$\mathcal{F}(x) = \sum_k \bar{\mathcal{W}}^k(x) \mathcal{I}_k(x) \quad (12)$$

where  $\mathcal{I}_k$  symbolizes the input ( $k$  is the index of the inputs) that is weighted by the normalized weight maps  $\bar{\mathcal{W}}^k$ . The normalization of the weights ensures that the intensity scale of the result is maintained in relatively the same scale as the inputs (since the sum of each pixel equals 1,  $\sum_k \bar{\mathcal{W}}^k(x) = 1$ ). The naive solution (please refer to figure 5) that directly implements this equation, introduces strong halos artifacts, mostly in the locations characterized by strong transitions of the weight maps. To prevent such degradation problems, we have opted for the adapted solution that employs a classical multi-scale pyramidal refinement strategy [46]. We also tested several



Fig. 5. The naive blending that directly implements equation 12 introduces halo artifacts, most apparent in locations characterized by strong transitions of the weight maps.

more recent edge preserving techniques (e.g. WLS [47]) but we did not obtain significant improvement. However, recent advanced methods need, in general, to tweak their parameters, as well as being more computationally intensive. In our case, each input  $\mathcal{I}_k$ , is decomposed into a pyramid by applying Laplacian operator at different scales. Similarly, for each normalized weight map  $\bar{\mathcal{W}}^k$ , a Gaussian pyramid is computed. Considering that both the Gaussian and Laplacian pyramids have the same number of levels, the mixing between the Laplacian inputs and Gaussian normalized weights is performed at each level independently, yielding the fused pyramid:

$$\mathcal{F}_l(x) = \sum_k G_l\{\bar{\mathcal{W}}^k(x)\} L_l\{\mathcal{I}_k(x)\} \quad (13)$$

where  $l$  represents the number of the pyramid levels (default value of the number of levels is  $l=5$ ) and  $L\{\mathcal{I}\}$  is the Laplacian version of the input  $\mathcal{I}$  while  $G\{\bar{\mathcal{W}}\}$  represents the Gaussian version of the normalized weight map of the  $\bar{\mathcal{W}}$ .

This step is performed successively for each pyramid layer, in a bottom-up manner. The final haze-free image  $\mathcal{J}$  is obtained by summing the contribution of the resulting inputs (levels of pyramid):

$$\mathcal{J}(x) = \sum_l \mathcal{F}_l(x) \uparrow^d \quad (14)$$

where  $\uparrow^d$  is the upsampling operator with factor  $d = 2^{l-1}$ . As a default characteristic, in our implementation the contribution of all the three weight maps is equally distributed.

## V. RESULTS AND DISCUSSION

To prove the robustness of our method, the new operator has been tested on a large dataset of different natural hazy images. Haze due to dust, smoke and other dry particles reduces visibility for distant regions by causing a distinctive gray hue in the captured images. However, our technique has been successfully tested as well for a slightly different case: foggy scenes (e.g. the first and the third example in figure 6; the reader is referred also to the supplementary material for more cases). For our problem, fog has a similar impact as haze, but technically it appears as a dense cloud of water droplets close to the ground when night conditions are clear but cold, and the heat released by the ground is absorbed during the day (please refer to figure 12). We assume that the input hazy/foggy images are color images and the images may contain achromatic objects.

As can be seen in figure 6, but also in figure 8, our operator is able to yield comparable and even better results

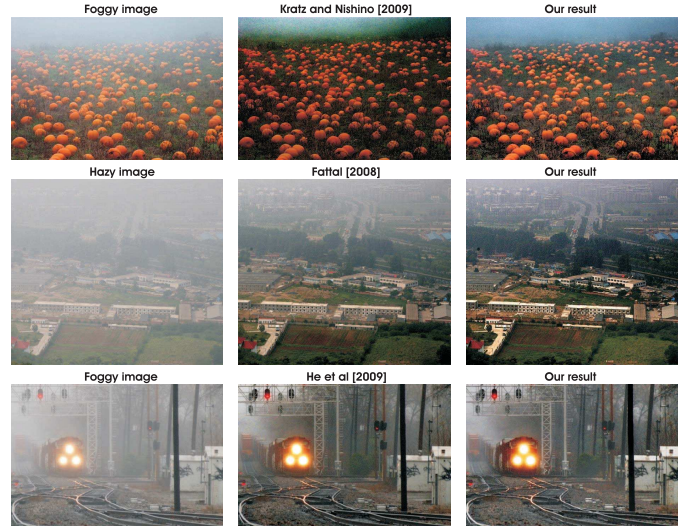


Fig. 6. Comparison with the single image dehazing techniques of Kratz and Nishino [9], Fattal [6], He et al. [8].

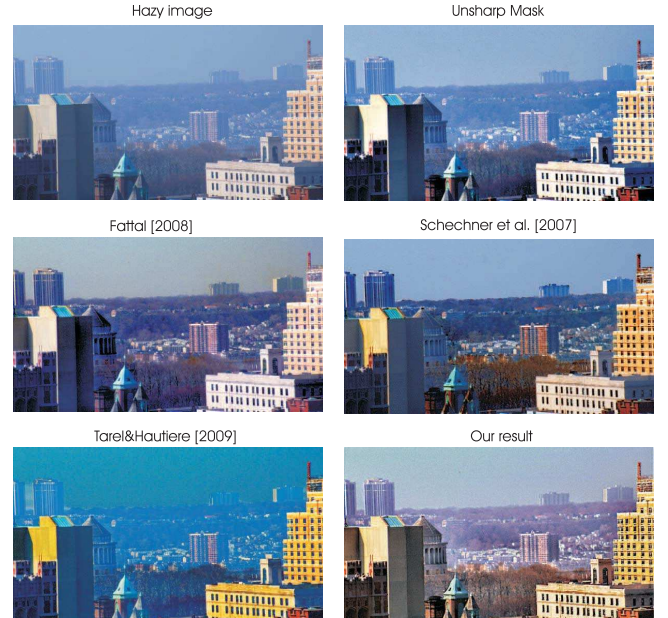


Fig. 7. A direct comparison between our result and the output of Schechner et al. [22] that is a polarization-based approach that employs two images (the worst and the best polarization states among the existing image versions). For this example our technique yields comparable result with Schechner et al. [22] and Fattal [6] while it outperforms unsharp mask and the specialized technique of Tarel and Hautière [10].

with more complex techniques. Compared with the techniques of Tan [7] and Tarel and Hautière [10] our technique is able to better preserve the fine transitions in the hazy regions without introducing unpleasing artifacts. Moreover, the technique of Tan [7] produces results with over-saturated colors. The recent technique of Kratz and Nishino [9] (recently extended in [14]) yields in general aesthetically pleasing results, but may introduce some artifacts in those regions considered to be at infinite depth (e.g. the skyline of the pumpkins field). Similarly, the technique of Fattal [6] performs well, but shows some limitations for situations with dense haze. This is mainly due to the fact that the method of



Fig. 8. Comparison of the recent dehazing techniques. Besides the initial hazy images in this figure are displayed the results of Tan [7], Fattal [6], Kopf et al. [4] and our technique. The reader is asked for a close inspection.

Fattal [6] is basically a statistic interpretation that requires variance to estimate the depth map. On the other hand, our technique yields visually similar results with the technique of He et al. [8]. However, by a closer analysis of the results, a difference can be observed between how colors are restored by the two methods, especially for the distant regions (e.g. in figure 8 the sky and the clouds have a different hue rendition). Also, the technique of He et al. [8], seems to restore slightly better the fine transitions of the regions closer to the horizon. However, our technique has the advantage of enhancing robustly such degraded images, without estimating the transmission, that needs to be refined by a computationally expensive alpha matting procedure in the approach of He et al. [8].

Figure 7 shows a direct comparison between our result and the output of Schechner et al. [22] that is a multi-image dehazing approach. Nevertheless, as can be seen, our single image dehazing operator is able to produce comparable results with the technique of Fattal [6] but also with the method of Schechner et al. [22]. The technique of Schechner et al. [22] is a polarization-based approach that employs two images - the worst and the best polarization states among the existing image versions. In this case, we processed only one input of those provided by Schechner et al. [22]. Moreover, for this example our technique outperforms unsharp mask and the specialized technique of Tarel and Hautière [10].

Partially, these observations are strengthened by analyzing the gradient distribution of the considered techniques in figures 9, 11. For the high resolution versions of

these images and several additional results, please refer to <http://research.edm.uhasselt.be/cancuti/Supplementary.zip>.

In figure 8 is presented direct comparisons against the recent dehazing techniques. In addition to the most representative recent single image dehazing techniques of Tan [7], Fattal [6], He et al. [8], Tarel and Hautière [10], Nishino et al. [14], we analyzed the technique of Kopf et al. [4] that uses a rough 3D map approximation of the scene. Based on these results we perform a quantitative evaluation using the blind measure of Hautière et al. [13]. Basically, this quality assessment approach consists in computing the ratio between the gradients of the image before and after restoration. This is based on the concept of visibility level, commonly used in lighting engineering. In table I we considered four images (named as **ny12**, **ny17**, **y01** and **y17**), where indicator  $e$  represents edges newly visible after restoration, indicator  $\bar{r}$  represents the mean ratio of the gradients at visible edges, while indicator  $\Sigma$  represents the percentage of pixels which become completely black or completely white after restoration. To compute this indicator we used the parameters used in [10]. Besides the aforementioned dehazing techniques, the values of these indicators when applying just an unsharp filter are shown in the table.

Analyzing the results of table I, in general, all the considered techniques (including our technique) yield small values of the  $\Sigma$  descriptor (the percentage of pixels which become completely black or completely white after the restoration). On the other hand, indicator  $e$  shows that most of the methods depending on the processed image remove some of the

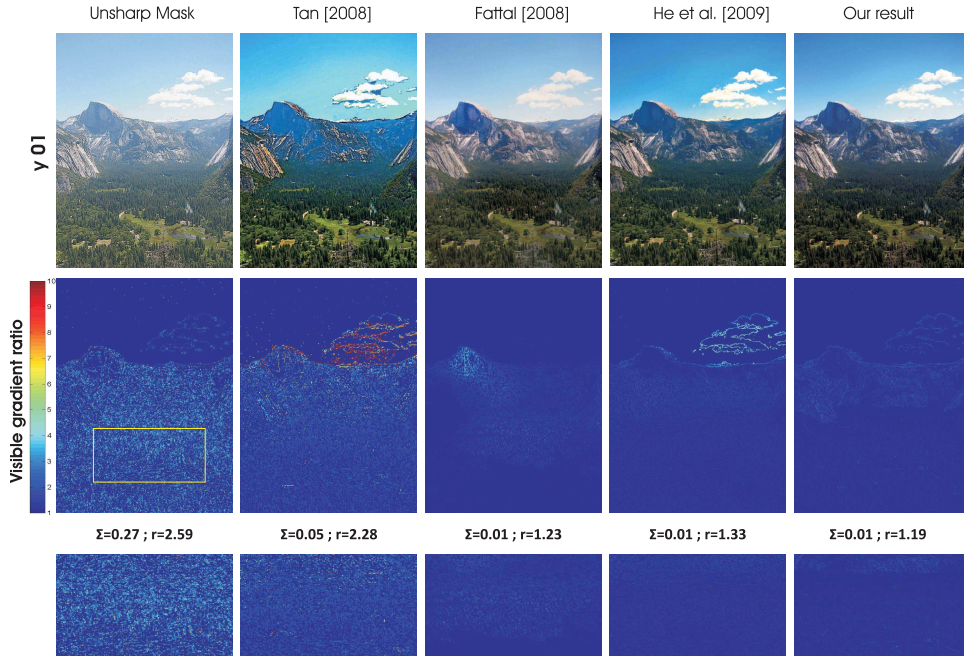


Fig. 9. Interpretation of the indicator  $\bar{r}$  proposed by Hautière et al. [13]. Except *unsharp mask filter* the analyzed methods yield low values of  $\Sigma$  (the percentage of pixels that becomes completely white or black after restoration). In general, methods that increase too much the local contrast are characterized by high values of indicator  $\bar{r}$ . This is demonstrated by the results shown in this figure and figure 11, supported also by the values shown in table 1. As an example, the method of Tan [7] adds some extra edges in the horizon region. We believe that for a more objective evaluation additional characteristics need to be taken into account (e.g. relation between depth and gradients, the amplitude of gradients, the reversal of the gradients).

visible edges. Interestingly, only our method and He et al. [8] technique, are characterized by positive values of the indicator  $e$  for the considered images.

Moreover, regarding indicator  $\bar{r}$ , the measure produces small values of indicator  $\bar{r}$  (the ratio of the gradient norms after and before restoration) for our results. Since one may observe that the appearance in our case is globally restored and the value of indicator  $\bar{r}$  is kept close to the minimum value ( $\bar{r} = 1$ ), one may deduce that in our case the local contrast was restored moderately. This feature is achieved also by the methods of Fattal [6], He et al. [8] and Kopf et al. [4]. On the other hand, the techniques of Tarel and Hautière [10] and Tan [7] increase too strongly the local contrast and as a result these approaches have higher values of indicator  $\bar{r}$ . Regarding indicator  $\bar{r}$ , the first group of techniques demonstrates less spurious edges and artifacts. Analyzing images of figure 9 that displays results processed by unsharp mask, Tan [7], Fattal [6], He et al. [8] and our approach, one may observe that in general the techniques with low values of indicator  $\bar{r}$  show less spurious edges and artifacts.

To the best of our knowledge, the blind measure of Hautière et al. [13] is the only existing method designed to give a quantitative interpretation for dehazing operation. The indicators of this measure are able to reveal only partially the level of restoration and degradation. Obviously, for a more objective evaluation additional characteristics need to be taken into account (e.g. relation between depth and gradients, the amplitude of gradients, the reversal of the gradients). For example, after restoration, gradients that were not visible should be emphasized, and that effect needs to be proportional to the distance from the camera. One would expect

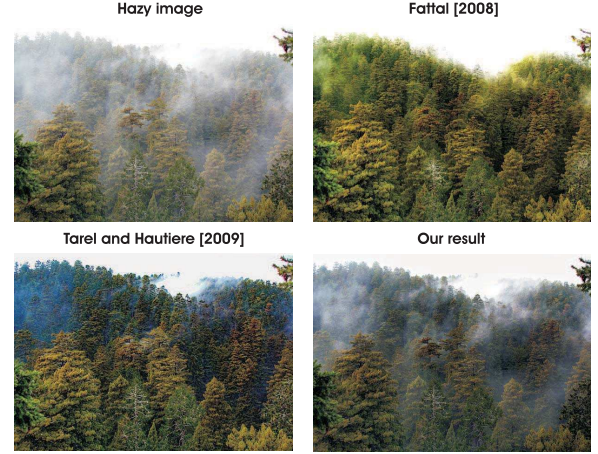


Fig. 10. Our technique is limited to homogeneous hazy images.

to see a stronger *visible gradient ratio* as one goes further away (towards the top of the image). While, the method of Tan [7] yields a too strong emphasis of the gradients, the results of physically-based methods such as Kopf et al. [4], Nishino [14] and also our results demonstrate edge enhancements that are consistent with the depth variation. Interestingly, the results of the method by Fattal [6] are characterized by stronger gradients for near scene points while the results of He et al. [8] present in some cases a very non-linear emphasis of the gradients.

To conclude, by a simple visual inspection of the results in figures 9 and 11, our technique is shown to be less prone to artifacts, yielding results similar to the physically-based techniques of He et al. [8], Fattal [6], Kopf et al. [4] and

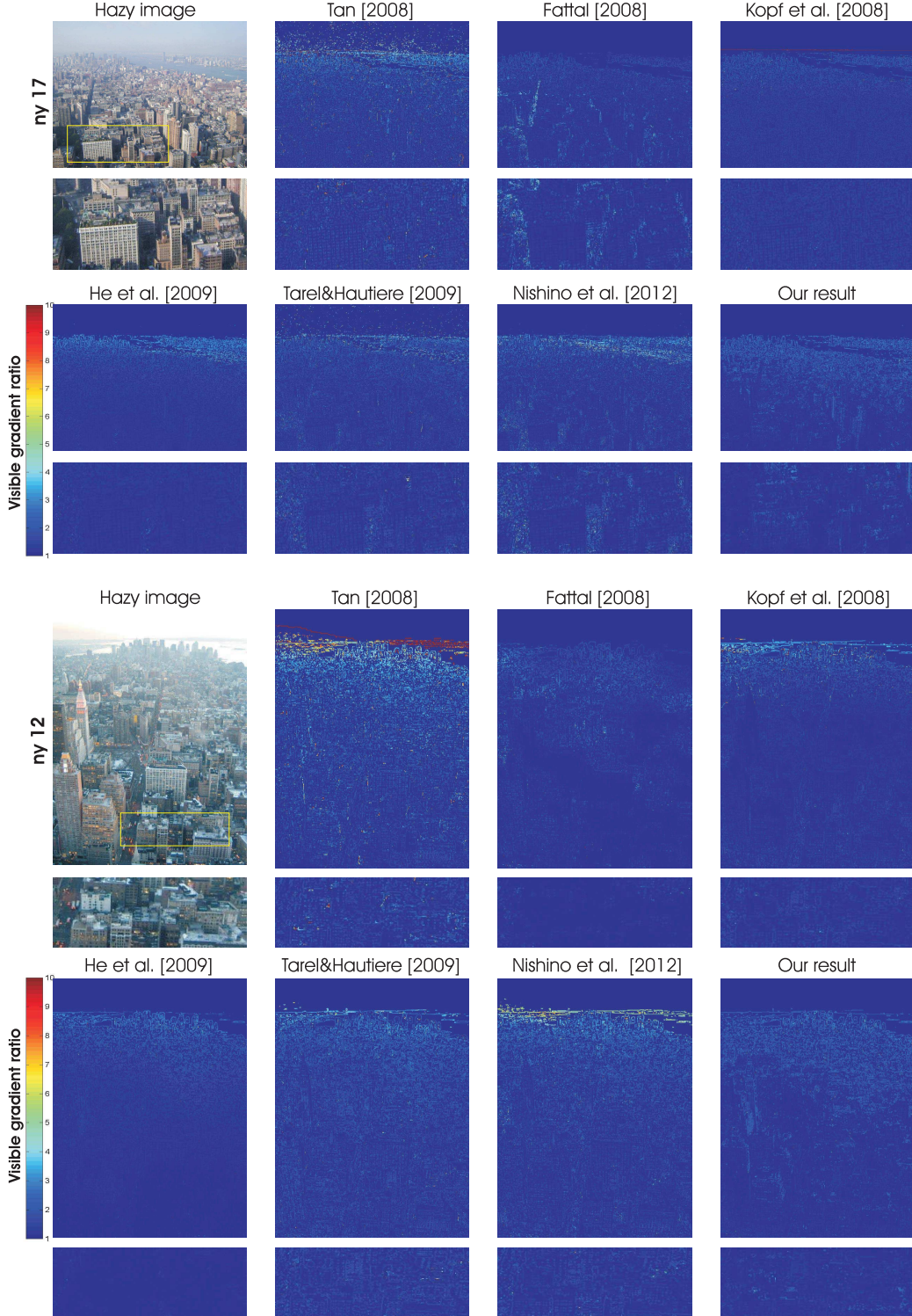


Fig. 11. Comparison of the analyzed dehazing techniques based on the indicator  $\bar{r}$  proposed by Hautière et al. [13]. To better visualize the restoration but also the level artifacts introduced by different techniques a cropped region is shown below.

Nishino et al. [14]. This is a key advantage of our technique, since we do not explicitly estimate the depth, while our method is much faster and simple than the other approaches that yield similar outputs. Moreover, it can be observed that the techniques of Tan [7] and Tarel and Hautière [10] restore some non-existent gradients.

Furthermore, compared with most of the existing techniques, an important advantage of our strategy is required computation time, since our method is able to process a  $600 \times 800$  image in approximately 2–300 ms (20% for derived inputs, 35% for the weight maps while the multi-scale strategy takes approximately 45% of the entire fusion process on an

TABLE I  
QUALITATIVE COMPARISON OF THE FOUR IMAGES (**ny12**, **ny17**, **y01** AND **y17**) SHOWN IN FIGURE 8  
BASED ON THE INDICATORS  $\Sigma$  AND  $\bar{r}$  OF HAUTIÈRE *et al.* [13].

	unsharp mask			Tan [7]			Fattal [6]			Kopf [4]			He [8]			Tarel [10]			Nishino [14]			Ours		
	$e$	$\Sigma$	$\bar{r}$	$e$	$\Sigma$	$\bar{r}$	$e$	$\Sigma$	$\bar{r}$	$e$	$\Sigma$	$\bar{r}$	$e$	$\Sigma$	$\bar{r}$	$e$	$\Sigma$	$\bar{r}$	$e$	$\Sigma$	$\bar{r}$	$e$	$\Sigma$	$\bar{r}$
ny12	-0.09	0.72	2.57	-0.14	0.02	2.34	-0.06	0.086	1.32	0.05	0.00	1.42	0.06	0.0	1.42	0.07	0.0	1.88	-0.01	0.46	1.81	0.02	0.0	1.49
ny17	-0.10	1.28	2.29	-0.06	0.01	2.22	-0.12	0.02	1.56	0.01	0.01	1.62	0.01	0.00	1.65	-0.01	0.0	1.87	-0.07	0.91	1.79	0.12	0.0	1.54
y01	0.04	0.27	2.59	0.08	0.01	2.28	0.04	0.02	1.23	0.09	0.00	1.62	0.08	0.01	1.33	0.02	0.0	2.09	0.11	0.71	1.79	0.07	0.01	1.19
y16	0.09	2.32	1.87	-0.08	0.01	2.08	0.03	0.00	1.27	-0.01	0.00	1.34	0.06	0.00	1.42	-0.01	0.0	2.01	0.01	1.71	1.29	0.18	0.01	1.46



Fig. 12. More results generated for foggy scenes.

Intel Core i7 CPU, 8GB RAM). In comparison, the method of Tan [7] needs more than 5 minutes per image, He et al. [8] requires 20 seconds, Tarel and Hautière [10] technique takes less than 0.5 seconds, the method of Fattal [6] needs 35 seconds, while the processing times of the method [14] were not reported.

Even though the proposed method performs in general well, as the previous methods, a limitation of our algorithm may be observed for images that are characterized by non-homogeneous haze layers. Figure 10 depicts this issue. As can be seen, the other single image dehazing approaches present serious limitations while tackling this challenging case (e.g. the technique of Tarel and Hautière [10] yields unpleasing artifacts such as coarse edges and color distortion). Moreover, even though some enhancement may be achieved, our technique is limited to processing color images.

## VI. CONCLUSION

In this paper we have demonstrated that a fusion-based approach can be used to effectively enhance hazy and foggy images. To the best of our knowledge, this is the first fusion-based strategy that is able to solve such problems using only

one degraded image. We have shown that, by choosing appropriate weight maps and inputs, a multi-scale fusion strategy can be used to effectively dehaze images. Our technique has been tested on a large data set of natural hazy images. The method is faster than existing single image dehazing strategies and yields accurate results. In future work we would like to test our method on videos.

## REFERENCES

- [1] P. Chavez, "An improved dark-object subtraction technique for atmospheric scattering correction of multispectral data," *Remote Sens. Environ.*, vol. 24, no. 3, pp. 459–479, 1988.
- [2] G. D. Moro and L. Halounova, "Haze removal and data calibration for high-resolution satellite data," *Int. J. Remote Sens.*, pp. 2187–2205, 2006.
- [3] S. Narasimhan and S. Nayar, "Contrast restoration of weather degraded images," *IEEE Trans. Pattern Anal. Mach. Intell.*, vol. 25, no. 6, pp. 713–724, Jun. 2003.
- [4] J. Kopf, B. Neubert, B. Chen, M. Cohen, D. Cohen-Or, O. Deussen, M. Uyttendaele, and D. Lischinski, "Deep photo: Model-based photograph enhancement and viewing," *ACM Trans. Graph.*, vol. 27, no. 5, p. 116, 2008.
- [5] T. Treibitz and Y. Y. Schechner, "Polarization: Beneficial for visibility enhancement?" in *Proc. IEEE Conf. Comput. Vis. Pattern Recognit.*, Jun. 2009, pp. 525–532.
- [6] R. Fattal, "Single image dehazing," *ACM Trans. Graph., SIGGRAPH*, vol. 27, no. 3, p. 72, 2008.
- [7] R. T. Tan, "Visibility in bad weather from a single image," in *Proc. IEEE Conf. Comput. Vis. Pattern Recognit.*, Jun. 2008, pp. 1–8.
- [8] K. He, J. Sun, and X. Tang, "Single image haze removal using dark channel prior," in *Proc. IEEE Conf. Comput. Vis. Pattern Recognit.*, Jun. 2009, pp. 1956–1963.
- [9] L. Kratz and K. Nishino, "Factorizing scene albedo and depth from a single foggy image," in *Proc. IEEE Int. Conf. Comput. Vis.*, Sep.–Oct. 2009, pp. 1701–1708.
- [10] J.-P. Tarel and N. Hautiere, "Fast visibility restoration from a single color or gray level image," in *Proc. IEEE Int. Conf. Comput. Vis.*, Sep.–Oct. 2009, pp. 2201–2208.
- [11] C. O. Ancuti, C. Ancuti, and P. Bekaert, "Effective single image dehazing by fusion," in *Proc. IEEE Int. Conf. Image Process.*, Sep. 2010, pp. 3541–3544.
- [12] H. B. Mitchell, *Image Fusion: Theories, Techniques and Applications*. New York, NY, USA: Springer-Verlag, 2010.
- [13] N. Hautiere, J.-P. Tarel, D. Aubert, and E. Dumont, "Blind contrast enhancement assessment by gradient ratioing at visible edges," *J. Image Anal. Stereol.*, vol. 27, no. 2, pp. 87–95, 2008.
- [14] K. Nishino, L. Kratz, and S. Lombardi, "Bayesian defogging," *Int. J. Comput. Vis.*, vol. 98, no. 3, pp. 263–278, 2012.
- [15] Y. Zhang, B. Guindon, and J. Cihlar, "An image transform to characterize and compensate for spatial variations in thin cloud contamination of Landsat images," *Remote Sens. Environ.*, vol. 82, nos. 2–3, pp. 173–187, 2002.
- [16] S. Narasimhan and S. Nayar, "Vision in bad weather," in *Proc. IEEE Int. Conf. Comput. Vis.*, Sep. 1999, pp. 820–827.
- [17] S. Narasimhan and S. Nayar, "Chromatic framework for vision in bad weather," in *Proc. IEEE Conf. Comput. Vis. Pattern Recognit.*, Jun. 2000, pp. 598–605.

- [18] S. Narasimhan and S. Nayar, "Interactive de-wheathering of an image using physical models," in *Proc. IEEE Workshop Color Photometric Methods Comput. Vis.*, Oct. 2003, p. 1.
- [19] N. Hautiere, J.-P. Tarel, and D. Aubert, "Towards fog-free in-vehicle vision systems through contrast restoration," in *Proc. IEEE Conf. Comput. Vis. Pattern Recognit.*, Jun. 2007, pp. 1–8.
- [20] Y. Y. Schechner, S. Narasimhan, and S. Nayar, "Polarization-based vision through haze," *Appl. Opt.*, vol. 42, no. 3, pp. 511–525, 2003.
- [21] S. Shwartz, E. Namer, and Y. Schechner, "Blind haze separation," in *Proc. IEEE Conf. Comput. Vis. Pattern Recognit.*, 2006, pp. 1984–1991.
- [22] Y. Schechner and Y. Averbuch, "Regularized image recovery in scattering media," *IEEE Trans. Pattern Anal. Mach. Intell.*, vol. 29, no. 9, pp. 1655–1660, Sep. 2007.
- [23] E. Namer, S. Shwartz, and Y. Schechner, "Skyless polarimetric calibration and visibility enhancement," *Opt. Exp.*, vol. 17, no. 2, pp. 472–493, 2009.
- [24] A. Levin, D. Lischinski, and Y. Weiss, "A closed form solution to natural image matting," *IEEE Trans. Pattern Anal. Mach. Intell.*, vol. 30, no. 2, pp. 228–242, Feb. 2008.
- [25] A. Agarwala, M. Dontcheva, M. Agrawala, S. M. Drucker, A. Colburn, B. Curless, D. Salesin, and M. F. Cohen, "Interactive digital photomontage," *ACM Trans. Graph., SIGGRAPH*, vol. 23, no. 3, pp. 294–302, 2004.
- [26] P. Perez, M. Gangnet, and A. Blake, "Poisson image editing," *ACM Trans. Graph., SIGGRAPH*, vol. 22, no. 3, pp. 313–318, 2003.
- [27] R. Brinkmann, *The Art and Science of Digital Compositing*. San Mateo, CA, USA: Morgan Kaufmann, 1999.
- [28] M. Grundland, R. Vohra, G. P. Williams, and N. A. Dodgson, "Cross dissolve without cross fade: Preserving contrast, color and salience in image compositing," *Comput. Graph. Forum*, vol. 25, no. 3, pp. 577–586, 2006.
- [29] P. J. Burt, K. Hanna, and R. J. Kolczynski, "Enhanced image capture through fusion," in *Proc. IEEE Int. Conf. Comput. Vis.*, May 1993, pp. 173–182.
- [30] T. Mertens, J. Kautz, and F. V. Reeth, "Exposure fusion: A simple and practical alternative to high dynamic range photography," *Comput. Graph. Forum*, vol. 28, no. 1, pp. 161–171, 2009.
- [31] L. Schaul, C. Fredembach, and S. Süsstrunk, "Color image dehazing using the near-infrared," in *Proc. IEEE Int. Conf. Image Process.*, Nov. 2009, pp. 1629–1632.
- [32] E. J. McCartney, *Optics of the Atmosphere: Scattering by Molecules and Particles*. New York, NY, USA: Wiley, 1976.
- [33] H. Koschmieder, "Theorie der horizontalen sichtweite," in *Beiträge zur Physik der Freien Atmosphäre*. Munich, Germany: Keim & Nemnich, 1924.
- [34] G. Buchsbaum, "A spatial processor model for object colour perception," *J. Franklin Inst.*, vol. 310, no. 1, pp. 1–26, 1980.
- [35] E. Land and J. McCann, "Lightness and retinex theory," *J. Opt. Soc. Amer. A*, vol. 61, no. 1, pp. 1–11, 1971.
- [36] V. Cardei, B. Funt, and K. Barnard, "Estimating the scene illumination chromaticity by using a neural network," *J. Opt. Soc. Amer. A*, vol. 19, no. 12, pp. 2374–2386, 2002.
- [37] G. Finlayson and E. Trezzi, "Shades of gray and colour constancy," in *Proc. 12th Color Imag. Conf.*, 2004, pp. 37–41.
- [38] J. van de Weijer, T. Gevers, and A. Gijsenij, "Edge-based color constancy," *IEEE Trans. Image Process.*, vol. 16, no. 9, pp. 2207–2214, Sep. 2007.
- [39] M. Ebner, *Color Constancy*, 1st ed. New York, NY, USA: Wiley, 2007.
- [40] A. Gijsenij and T. Gevers, "Color constancy using natural image statistics and scene semantics," *IEEE Trans. Pattern Anal. Mach. Intell.*, vol. 33, no. 4, pp. 687–698, Apr. 2011.
- [41] J. van de Weijer and T. Gevers, "Color constancy based on the grey-edge hypothesis," in *Proc. IEEE Int. Conf. Image Process.*, Sep. 2005, pp. 722–725.
- [42] J. K. Tsotsos, S. M. Culhane, W. Y. K. Wai, Y. Lai, N. Davis, and F. Nuflo, "Modeling visual attention via selective tuning," *Artif. Intell.*, vol. 78, nos. 1–2, pp. 507–545, 1995.
- [43] Y.-F. Ma and H.-J. Zhang, "Contrast-based image attention analysis by using fuzzy growing," in *Proc. 11th ACM Int. Conf. Multimedia*, 2003, pp. 374–381.
- [44] L. Itti, C. Koch, and E. Niebur, "A model of saliency-based visual attention for rapid scene analysis," *IEEE Trans. Pattern Anal. Mach. Intell.*, vol. 20, no. 11, pp. 1254–1259, Nov. 1998.
- [45] R. Achanta, S. Hemami, F. Estrada, and S. Süsstrunk, "Frequency-tuned salient region detection," in *Proc. IEEE Conf. Comput. Vis. Pattern Recognit.*, Jun. 2009, pp. 1597–1604.
- [46] P. Burt and T. Adelson, "The Laplacian pyramid as a compact image code," *IEEE Trans. Commun.*, vol. 31, no. 4, pp. 532–540, Apr. 1983.
- [47] Z. Farbman, R. Fattal, D. Lischinski, and R. Szeliski, "Edge-preserving decompositions for multi-scale tone and detail manipulation," in *Proc. ACM SIGGRAPH*, 2008, p. 67.

**Codruta Orniana Ancuti** is a Senior Researcher with Hasselt University, Hasselt, Belgium. She has been involved in academic research since 2005, having worked previously for Siemens VDO, Munich, Germany. After two years as a Researcher with the Human Computer Interaction Group, where she was involved in several research projects, she started the Ph.D. degree with the Vision Computing Group in 2011. She developed different state-of-the-art computational imaging algorithms covering subjects such as robust video and image decolorization, single image-dehazing and underwater image enhancement. Her current research interests include visually impaired substitution systems and computational photography.

**Cosmin Ancuti** received the M.S. degree in computer science from the University Politehnica of Timisoara, Timisoara, Romania, in 2003. He is a Senior Researcher with IMINDS - Hasselt University, Hasselt, Belgium. From 2002 to 2005, he was a Software Engineer with Siemens VDO, Munich, Germany. In 2005, he joined Hasselt University, Hasselt, Belgium, where he received the Ph.D. degree in 2009. He is the author of more than 35 papers published in international conference proceedings and journals. His current research interests include image/video enhancement techniques, computational photography, and low level computer vision.